Element-specific magnetic properties of mixed 3*d*-4*f* metallacrowns

A. Alhassanat,[1] C. Gamer,[2] A. Rauguth,[2] A. A. Athanasopoulou,[2] J. Sutter,[2] C. Luo,[3,4] H. Ryll,[3] F. Radu,[3] A. A. Sapozhnik,[1] T. Mashoff,[1] E. Rentschler,[2] and H. J. Elmers[1,*]

[1]*Institut für Physik, Johannes Gutenberg-Universität, Staudingerweg 7, D-55099 Mainz, Germany*

[2]*Institut für Anorganische und Analytische Chemie, Universität Mainz, D-55128 Mainz, Germany*

[3]*Helmholtz-Zentrum Berlin für Materialien und Energie, Albert-Einstein Str. 15, 12489, Berlin, Germany*

[4]*Institut für Experimentelle und Angewandte Physik, Universität Regensburg, Universitätsstrae 31, 93053 Regensburg, Germany*

(Received 27 March 2018; revised manuscript received 31 July 2018; published 31 August 2018)

Single molecule magnets comprising rare earth metals are of high interest due to the unquenched orbital moments of the rare earth ions that result in a large energy barrier for magnetization reversal. We investigate the magnetic properties of polynuclear 3*d*-4*f* 15-MC-5 metallacrowns using x-ray magnetic circular dichroism of powder samples at a temperature of 7 K in a magnetic field of 7 T. The sum rule analysis reveals element-specific spin and orbital moments. The magnetic moments of the 3*d* transition metal Ni(II) ions are coupled antiferromagnetically to each other and contribute only little to the total molecular moment. The spin and orbital moments of the rare earth ions are unexpectedly smaller than the ionic values resulting from Hund's rules. We explain the reduction of the orbital magnetic moment by a finite magnetic anisotropy. Considering an energy functional including magnetic anisotropy and Zeeman energy the powder average reveals a magnetic anisotropy of 28 meV (340 K) in the case of Dy(III) and 7 meV (85 K) in the case of Tb(III). The spin moments agree with the ionic value, too, when the expectation values of the dipole operator are considered.

DOI: 10.1103/PhysRevB.98.064428

I. INTRODUCTION

Rare earth ions are promising components for molecular magnets. The 4*f* ions Tb(III) and Dy(III) show a large orbital magnetic moment in the ground state combined with a strong spin-orbit coupling. Thus they potentially enhance the molecular magnetic anisotropy leading to slow relaxation rates and single molecule magnet (SMM) behavior [1–6]. Molecular structures comprising Tb(III) or Dy(III) ions can exhibit magnetic anisotropy energies of single molecules that are on the order of the thermal energy at room temperature. Such a high energy barrier for magnetization reversal provides an important precondition for single molecule magnets [7–10]. Mononuclear phtalocyaninate [11], polyoxometalate [12,13], organometallic [14–16], or purely inorganic lanthanide compounds [17] are reported to possess high anisotropy energies leading to SMM properties. Recently, polynuclear SMMs providing further flexibility in tuning the magnetic properties came back into the focus of research. The synthesis of polynuclear 4*f* clusters has led to high energy barriers up to 530 K [18–22]. Some heteronuclear 3*d*-4*f* SMMs [23–27] have been synthesized with anisotropy barriers comparable to those for 3*d*-only SMMs.

Metallacrowns are an interesting group of multinuclear cyclic metal clusters, with a structure comparable to the organic crown ethers consisting of -[M-N-O]- repeated units. Metallacrowns possess a high thermodynamic stability and integrity in solution. Depending on the magnetic anisotropy of the metal ions composing the ring or being encapsulated, single molecule magnet behavior is observed [28–30]. The inclusion of 4*f* elements in metallacrowns is promising for achieving the desirable large anisotropy. In this case, the interaction between the single-ion electron density and the crystal field leads to a large single-ion anisotropy [31]. Understanding the particular crystal field environment that results in large anisotropies is important for the optimization of the slow relaxation properties in metallacrowns.

The understanding of magnetic properties of 4*f*-containing molecules is challenging [27] because of the presence of large orbital moments. In 3*d* transition metal clusters comprising only one species of ions intramolecular coupling values result from the temperature dependence of the magnetic susceptibility. In contrast, 3*d*-4*f* molecules can hide the intramolecular coupling under the dominant effect of ligand-field splittings [32]. Moreover, the ground state total angular momentum may depend in this case on the ligand field [33,34]. X-ray magnetic circular dichroism (XMCD) provides element-specific information and thus helps to understand the complex magnetic behavior of 3*d*-4*f* magnetic molecules [35–48]. In particular, molecular magnetic anisotropy measurements on rare earth ions using XMCD have been reported in Ref. [49].

The study of element-specific magnetic properties of the homo- and heterometallic metallacrowns Cu(II) [12-$MC_{TM(Shi)}$-4] [TM=Cu(II), Fe(III), in short $CuCu_4$ and $CuFe_4$ [50,51] revealed a strongly different magnetization distribution. The $CuFe_4$ metallacrown shows a ratio between the Cu and Fe moment of -0.11. Instead, for $CuCu_4$ the magnetic moment is localized at the central Cu(II) ion. These results emphasized the importance of element-specific information on the magnetic properties of metallacrowns.

In this study we replace the central ion within a metallacrown scaffold by a rare earth (RE) ion. The larger size

*elmers@uni-mainz.de

of the RE(III) ion requires an extension of the ring size to five transition metal units surrounding the central RE(III) ion in order to keep the flat geometry of the magnetic cores. These molecules are classified as 15-MC-5 metallacrowns, describing the ring size and the number of oxygen atoms coordinating the encapsulated central ion. The RE(III) ion is surrounded by 5 Ni(II) ions in an almost planar ring-shaped configuration. In this article, we show how quantitative information on the magnetic single ion anisotropy is gained from the element-specific spin and orbital moments resulting from a sum rule analysis of the x-ray absorption spectra.

II. EXPERIMENT

RE[15-$MC_{Ni(II)N(picha)}$-5](μ-NO_3)(η^1-NO_3)$(py)_8$ (in short {$RENi_5$}) molecules with RE=Sm, Tb, and Dy have been synthesized as described in Ref. [52]. Magnetometry measurements were performed using a superconducting quantum intereference device (SQUID) magnetometer on powder material from the identical batch that was used for the x-ray absorption experiments. (See Fig. 1.)

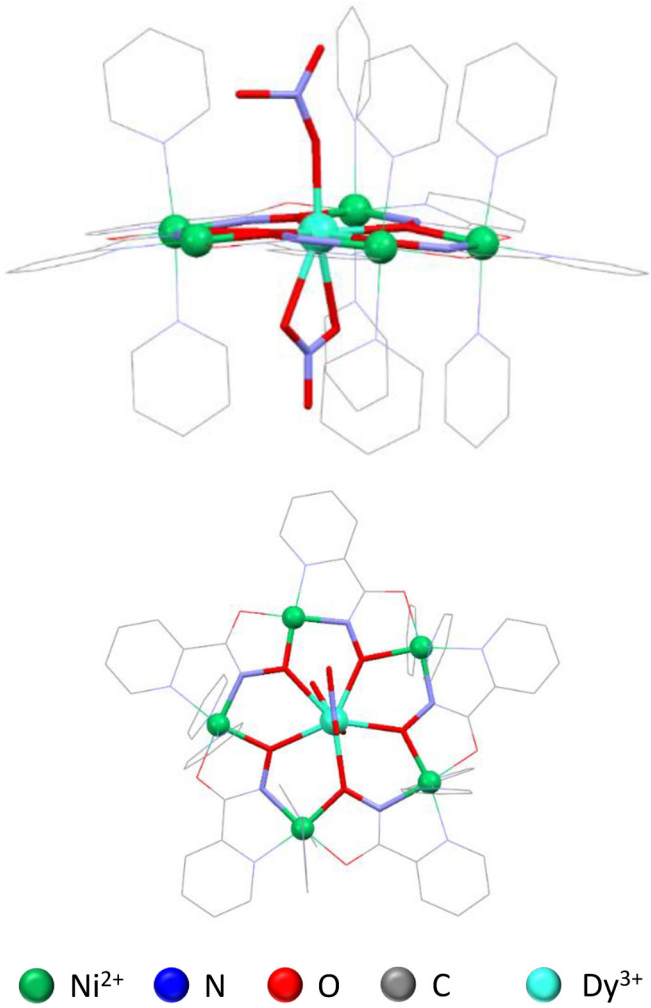

FIG. 1. Molecular structure of the Dy(III)[15-$MC_{Ni(II)N(picha)}$-5](μ_2-NO_3)(η^1-NO_3)$(py)_8$ ({$DyNi_5$}) molecule.

XMCD measurements were carried out at the VEKMAG endstation of the PM2 beamline at BESSY II [53]. For the XMCD measurements the {$RENi_5$} molecules were dissolved in methanol. Electrospray injection mass spectrometry confirms the structural and chemical integrity of the molecules after dissolving in methanol. The solution was thus drop cast on a rinsed Si waver surface. The solvent then rapidly evaporates under ambient conditions within minutes after the drop cast. The molecules form small randomly oriented microcrystals on the surface. With applying ultrahigh vacuum, no liquid remains on the sample surface. The purpose of solving and recrystallization in the rinsed Si surface is to minimize the crystal size and to have each small crystal be attached by van der Waals forces to the Si surface in order to prevent electrical charging during the measurement. Scanning electron microscopy images and x-ray diffraction data are fully in agreement with the random orientation of the deposited molecules. However, we cannot completely exclude a nonrandom orientation of the molecules deposited by drop cast, because monolayer coverages on the substrate may significantly contribute to the absorption signal but do not show up in the diffraction intensity.

X-ray absorption spectra (XAS) at the Ni $L_{3,2}$ and RE $M_{5,4}$ edges result from the total electron yield as measured by the sample current at 7 K. A magnetic field of 7 T was applied parallel and antiparallel to the incident photon beam with the sample oriented perpendicular to the magnetic field. The polarization degree is $P = 0.77$ at the Fe L edge. A calibration measurement at the Gd M edges confirms that the degree of polarization does not change within the experimental error of 3% within the photon energy range used for the present experiments. The polarization value has been considered for the evaluation of the sum rules (see below). We measured each spectrum twice in order to confirm that the x-ray beam does not damage the molecules. Even after several hours of absorption measurements we did not detect any changes of the spectra indicating that no radiation damage of the molecules occurred.

Spectra acquired with positive and negative field direction have been normalized at the preedge. The normalization accounts for a systematic field dependent detection efficiency of the radiation detector used for measuring the incident photon intensity. A linear function fitted to the pre- and postedge has been subtracted from the spectra acquired for opposite field direction in order to account for the background intensity caused by x-ray absorption in states with smaller binding energy.

Element-specific magnetic moments were determined by the sum rule analysis [54,55]. We have set the number of d holes to the values as determined by charge transfer multiplet calculations [56] and the number of f holes to the ionic values. The jj mixing effect is considered as a correction factor for the magnetic spin moment. The correction factor is 1 within the error limits in the case of the Ni(II) and Gd(III), Tb(III), and Dy(III), while it deviates in the case of the less than half-filled $4f$ shells [57]. The correction factor of 2.3 in the case of Sm(III) as reported in Ref. [58] has been considered for the quantitative evaluation.

The expectation value of the dipole operator $T_z = \langle \mathbf{T}_z \rangle$ [59] contributes to the effective spin moment for transition metal and rare earth ions. T_z only vanishes in the case of Gd(III)

and Eu(II). In contrast, T_z is large in the case of Sm(III), Tb(III), and Dy(III) (see Refs. [54,55]). In this case it can be calculated exactly according to Ref. [54]. The angular dependence of T_z can be described by the Legendre polynomial $(1 - 3\cos^2\theta)$ [60], which has been experimentally confirmed by Stepanow *et al.* [61] for the case of ordered Cu-phthalocyanine monolayers on Ag(100). An important precondition for the occurrence of this angular dependence is that the quadrupolar charge distribution remains largely unaffected by the magnetic spin orientation. This precondition is likely fulfilled in our case because the spin-orbit coupling is smaller than the bandwidth for the valence states of $3d$ and $4f$ metal ions but in principle it has to be tested by angular dependent measurements. The quadrupolar charge distribution results in $\langle T_x\rangle + \langle T_y\rangle + \langle T_z\rangle = 0$: the spin moment can be determined by averaging experiments where the spin is aligned along the x, y, and z axis. Alternatively, T_z vanishes for a magic angle orientation. In the case of a saturated magnetic state, i.e., for the external fields being much larger than the magnetic anisotropy fields, T_z vanishes for powder samples (see Ref. [61,62]). In contrast, for an external field much smaller than the magnetic anisotropy field, the exact result of T_z for RE(III) ions can be used to determine the spin moment [27]. The intermediate case of anisotropy and external fields being of equal size is discussed in Sec. IV.

III. RESULTS

Figure 2 shows the XAS and XMCD spectra of the $\{RENi_5\}$ samples for RE = Sm(III), Tb(III), and Dy(III). The Ni L_3 edge at a photon energy of 855 eV reveals a small additional satellite peak at 2 eV higher than the energy of the absorption maximum. Its intensity slightly decreases with increasing atomic number of the RE(III) ion indicating a change of the ligand field strength. Instead, the Ni L_2 edge at 870 eV shows a single peak. These features are characteristic for a Ni(II) ion within an octahedral ligand field. The RE XAS and XMCD spectra, shown in Fig. 2, probe the unoccupied $4f$ states. The larger absorption maximum at lower photon energy corresponds to the M_5 edge and the peak at higher photon energy indicates the M_4 edge. The spectra reveal the typical features for the RE(III) ions depending only marginally on the ligand field, reflecting the localized character of the $4f$ states that are not involved in the chemical bonding. The XMCD spectra (Fig. 2) directly reveal the parallel orientation of the Tb(III), Dy(III), and Ni(II) magnetic moment, indicated by the negative sign of the corresponding L_3 and M_5 XMCD maximum. In the case of Sm(III), instead, the Sm(III) spin moment shows antiparallel to the external field and to the Ni(II) moment, indicating an antiferromagnetic alignment in high fields of the spin moments of Ni(II) and Sm(III).

First, we discuss the magnetic moments of the Ni(II) ions. Taking into account the dipole selection rules, the sum rules result in magnetic spin and orbital moments [55]:

$$\mu_{\text{spin}}^{\text{eff}} = -\frac{3n_h\mu_B}{P}\frac{\int_{L3}\mu_{\text{MCD}}dE - 2\int_{L2}\mu_{\text{MCD}}dE}{\int_{L3+L2} I_{\text{iso}}dE},$$
$$\mu_{\text{orb}} = -\frac{3n_h\mu_B}{P}\frac{\int_{L3+L2}\mu_{\text{MCD}}dE}{\int_{L3+L2} I_{\text{iso}}dE}, \quad (1)$$

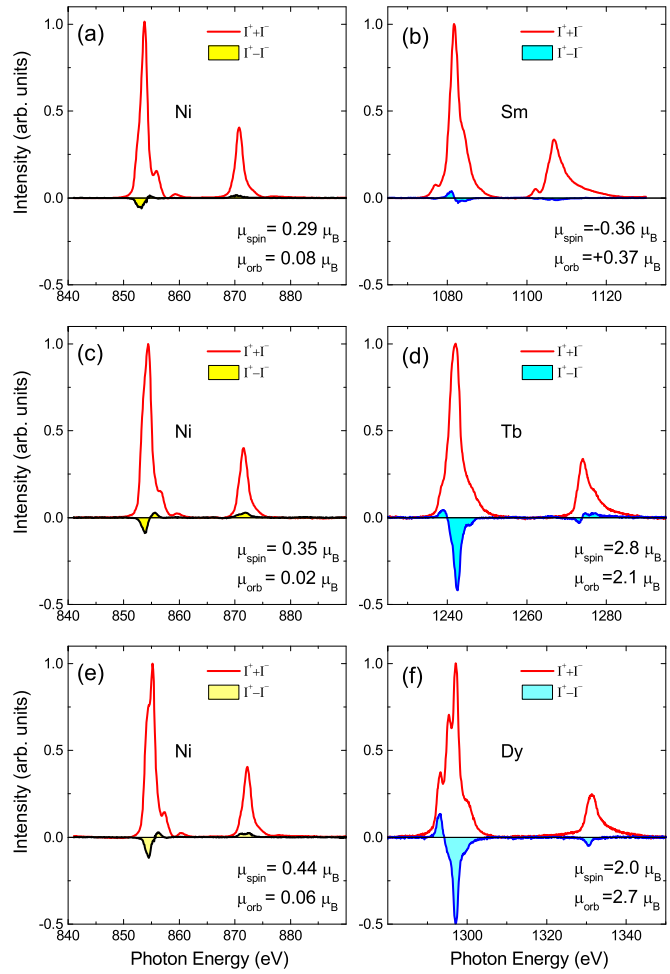

FIG. 2. X-ray absorption $I^+ + I^-$ and XMCD spectra $I^+ - I^-$ measured at the Ni $L_{3,2}$ and RE $M_{5,4}$ edges for the $\{RENi_5\}$ 15-MC-5 metallacrowns, (a),(b) for $\{SmNi_5\}$, (c),(d) for $\{TbNi_5\}$, and (e),(f) for $\{DyNi_5\}$, respectively. I^+ and I^- denote the total photoemission yield measured for external field parallel and antiparallel to the circular polarization vector of the synchrotron light. The step function resulting from transitions into continuum states has been subtracted from the sum intensity $I^+ + I^-$. The external field is ± 7 T and the temperature 7 K.

where $\mu_{\text{MCD}} = I^+ - I^-$ denotes the XMCD signal, $I_{\text{iso}} = I^+ + I^0 + I^-$ is the isotropic absorption signal, and $P = 0.77$ is the x-ray polarization. I^0 can be approximated by $I^0 = (I^+ + I^-)/2$. For Ni(II) the number of d holes is close to $n_h = 2$. The effective spin moment deviates from the spin moment μ_{spin} according to $\mu_{\text{spin}}^{\text{eff}} = \mu_{\text{spin}} + 7T_z\mu_B$. In the case of transition metal ions the T_z term depends on the chemical bonding and cannot be calculated exactly. It has been shown that it may assume large values for adsorbed Cu-phthalocyanine molecules [61]. In our case, the ligand field geometry is predominantly octahedral, tentatively leading to a smaller T_z term. Moreover, the magnetic anisotropy is expected to be small in view of the almost quenched orbital magnetic moments. Therefore, the T_z contribution vanishes for a powder sample because of the averaging over all possible orientations, i.e., $\mu_{\text{spin}}^{\text{eff}} = \mu_{\text{spin}}$.

TABLE I. Effective spin moment $\mu_{\text{spin}}^{\text{eff}}$ and orbital moment μ_{orb} in units of Bohr magnetons μ_{B} as determined by the sum rules for $\{\text{RENi}_5\}$ at 7 K for a field of 7 T. Saturation values for spin $\mu_{\text{spin}}^{*}/\mu_{\text{B}}$ and orbital magnetic moments $\mu_{\text{orb}}^{*}/\mu_{\text{B}}$ of the rare earth ions result from the model explained in the text. The molecular moment μ_{mol} calculated from the XMCD results are compared to the magnetization measured by superconducting quantum interference device (SQUID) magnetometry for the same temperature and magnetic field. The statistical error of sum rules values given in the table is in most cases less than 10%. The total error is dominated by systematic errors of the common factors polarization, n_h, and the error due to subtraction of transitions into continuous states. We estimate the total error to be on the order of 20%.

	Ni(II)		RE(III)				Mol. moments	
	$\mu_{\text{spin}}^{\text{eff}}$	μ_{orb}	$\mu_{\text{spin}}^{\text{eff}}$	μ_{orb}	μ_{spin}^{*}	μ_{orb}^{*}	μ_{mol}	μ_{SQUID}
$\{\text{SmNi}_5\}$	0.29(2)	0.08(1)	−0.8(2)	0.8(2)				1.2
$\{\text{TbNi}_5\}$	0.35(2)	0.02(1)	2.8(2)	2.1(1)	6.2(6)	3.0	8.4(6)	5.3
$\{\text{DyNi}_5\}$	0.44(3)	0.06(1)	2.0(2)	2.7(1)	6.0(6)	5.0	8.2(6)	5.9

The Ni spin moment increases slightly from $0.3\mu_{\text{B}}$ for $\{\text{SmNi}_5\}$ to $0.4\mu_{\text{B}}$ in the case of $\{\text{DyNi}_5\}$. The orbital magnetic moment amounts to a value of 10% of the spin moment, except for the case of $\{\text{SmNi}_5\}$ (30%).

In complexes with significant ligand fields it is *a priori* not clear if Hund's rules are obeyed. The branching ratio of the intensities $I(L_3)$ and $I(L_2)$ of the two spin-orbit split $2p$ absorption edges may give a hint at the spin state [63]. In our case the ratio amounts to $I(L_3)/[I(L_2)+I(L_3)] = 0.72$, in agreement with a high-spin state. The high-spin state also agrees with the fact that five- and sixfold coordinate Ni(II) typically shows high spin configuration. In the present case, one of the Ni(II) ions is fourfold coordinated and could indeed be low spin. Thus the spin state for four out of five Ni(II) ions is expected to be $S = 1$ and the corresponding spin moment should be close to the saturated value of $2\mu_{\text{B}}$. Instead, the observed spin moment is considerably smaller. This fact indicates an antiferromagnetic exchange coupling between the Ni spin moments.

In the case of the RE $3d \rightarrow 4f$ transitions the sum rules are

$$\mu_{\text{spin}}^{\text{eff}} = -\frac{3n_h\mu_{\text{B}}}{P}\frac{\int_{M5}\mu_{\text{MCD}}dE - \frac{3}{2}\int_{M4}\mu_{\text{MCD}}dE}{\int_{M5+M4} I_{\text{iso}}dE},$$
$$\mu_{\text{orb}} = -\frac{3n_h\mu_{\text{B}}}{P}\frac{\int_{M5+M4}\mu_{\text{MCD}}dE}{\int_{M5+M4} I_{\text{iso}}dE}, \quad (2)$$

For Sm, Tb, and Dy the numbers of unoccupied $4f$ states are $n_h = 9$, 6, and 5. In general, the effective spin moment comprises the true spin moment and a contribution from the expectation value of the dipole moment operator T_z, $\mu_{\text{spin}}^{\text{eff}} = \mu_{\text{spin}} + 6T_z\mu_{\text{B}}$. The contribution of T_z can in this case not be neglected and will be discussed below.

The results from the sum rule analysis are summarized in Table I. For an external field $B = 7$ T and temperature $T = 7$ K the Zeeman energy is much larger than the thermal energy, at least in the case of Tb and Dy. Therefore, one does not expect a strong temperature dependence, which is confirmed by field-dependent measurements using SQUID magnetometry.

Figure 3 shows the molecular magnetic moment $\mu_{\text{SQUID}}(H, T)$ as a function of external field for temperatures in the range of 2 K to 10 K. $\{\text{SmNi}_5\}$ shows a temperature-independent paramagnetic behavior. $\{\text{TbNi}_5\}$ and $\{\text{DyNi}_5\}$ reveal a linear increasing magnetic moment for small fields with a slope strongly dependent on temperature. For larger

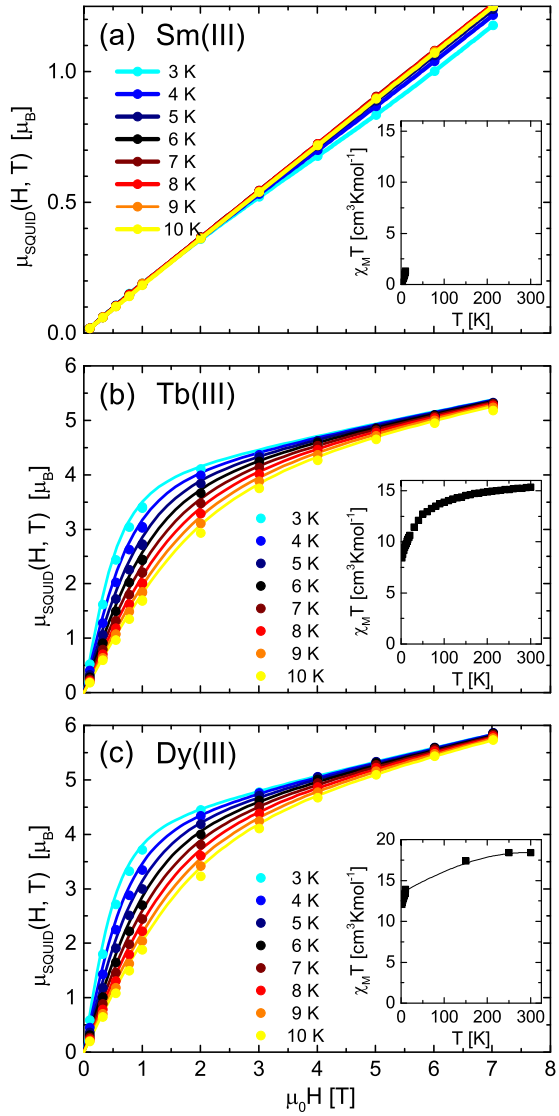

FIG. 3. Molecular magnetic moment $\mu_{\text{SQUID}}(H, T)$ as a function of external field for temperatures in the range of 3 K to 10 K (dots). (a) Data for $\{\text{SmNi}_5\}$. Full lines represent a guide to the eye. (b),(c) Data for $\{\text{TbNi}_5\}$ and $\{\text{DyNi}_5\}$, respectively. Thin lines in (b),(c) represent fits by a spin-Hamiltonian model with g and a temperature-independent paramagnetic component as fit parameter. The insets show experimental results for the magnetic susceptibility multiplied by temperature, χT.

fields $\mu_{\mathrm{SQUID}}(H,T)$ becomes temperature independent but does not saturate with increasing field.

IV. DISCUSSION

Neglecting exchange and anisotropy energies, one would expect ionic rare earth magnetic moments as observed for free RE(III) ions. With the assumption of a much larger LS coupling compared to the crystal field within the $4f$ shell one obtains, according to Hund's rules, for Sm(III) $2S=5,\ L=5$, for Tb(III) $2S=6,\ L=3$, and for Dy(III) $2S=5,\ L=5$. In the case of Sm and Dy one thus expects the same absolute values for spin and orbital moments of $5\mu_{\mathrm{B}}$; however, in the case of Sm spin and orbital moments are of opposite sign and thus partially compensate each other, whereas in the case of Dy the spin and orbital moments add up to $10\mu_{\mathrm{B}}$. The Tb spin moment, $6\mu_{\mathrm{B}}$, is twice as large as the orbital moment of $3\mu_{\mathrm{B}}$, adding up to a total ionic moment of $9\mu_{\mathrm{B}}$, which is almost as large as the Dy moment. In contrast, the experimentally determined spin as well as the orbital moments are considerably smaller. A strong magnetic anisotropy that forces the orbital magnetic moment along the molecular symmetry axis provides an obvious explanation for this observation. Due to the LS coupling, spin and orbital moments are aligned parallel to each other. For an infinitely strong magnetic anisotropy one expects an ensemble average over all molecular orientations in the powder sample, where only the component projected on the field axis is measured. This consideration would result in a measured moment of exactly half of the theoretical value.

For an intermediate value of the magnetic anisotropy the orientation of the rare earth magnetic moment results from the minimization of the free enthalpy:

$$g=-\mu^{*}_{\mathrm{RE}}B\,\cos\vartheta+K_{\mathrm{RE}}\cos^{2}(\theta-\vartheta), \tag{3}$$

with K_{RE} denoting the anisotropy constant and $\mu^{*}_{\mathrm{RE}}=\mu^{*}_{\mathrm{spin}}+\mu^{*}_{\mathrm{orb}}$ the corresponding absolute value of the magnetic moment of the rare earth ion. The angles θ and ϑ denote the angle of the molecular symmetry axis and of the magnetic moment direction with respect to the external field direction, respectively (see Fig. 4).

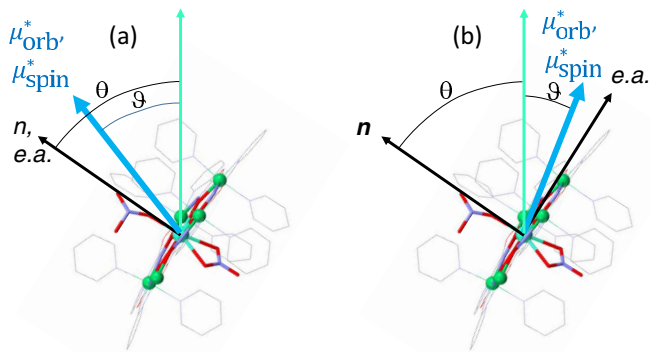

FIG. 4. Sketch of the magnetic moment orientation (blue) of the central rare earth ion with respect to the external field direction (green) and the molecular symmetry axis (black). The magnetic anisotropy is assumed to reveal a magnetic easy axis along the molecular symmetry axis (a) or an easy plane anisotropy (b) in the plane of the Ni(II) ions.

Please note that we have neglected the effective exchange energy between the rare earth and Ni spin moments. If the exchange constant was very large, the Ni moment would direct parallel to the rare earth moment and contribute to the Zeeman term. This contribution is, even for strong exchange coupling, only about 10% of the contribution from the rare earth magnetic moment. Furthermore, the $3d$-$4f$ exchange coupling is considered to be smaller than the thermal energy at 7 K (ca. 0.5 meV). In Ref. [27], for example, a value of 0.02 meV has been reported for the exchange coupling between Dy(III) and Cr(III). Reference [64] predicts an exchange interaction of 0.1 meV for Gd(III) and Ni(II) from density functional theory calculations. Therefore, we cannot totally exclude that the magnetic anisotropy may be partly due to exchange coupling between rare earth and transition metal ions. However, for the planar in the planar arrangement within the molecules investigated here and the RE(III)-Ni(II) ions being bridged by extended N-O linkers we do not expect considerable contributions. In our case $\chi T(T)$ (see Fig. 3) monotonously decreases with decreasing temperature. In the case of $3d$ metal clusters such a behavior indicates an intramolecular antiferromagnetic exchange coupling. However, for the case of rare earth ions comprising orbital angular momentum a similar temperature dependence can also be observed without exchange coupling [65].

For a given molecular orientation θ the orientation of the magnetic moment $\vartheta(r)$ exclusively depends on the ratio $r=K_{\mathrm{RE}}/\mu^{*}_{\mathrm{RE}}B$. We further assume a random orientation of the molecules in the sample and average over all possible orientations, resulting in the rare earth moment μ_{proj} projected on the field direction:

$$\mu_{\mathrm{proj}}(r)/\mu^{*}_{\mathrm{RE}}=\int_{0}^{\pi/2}\cos\vartheta(r)\sin\theta\,d\theta. \tag{4}$$

The result of this calculation is shown in Fig. 5(a). For $r=0$, i.e., vanishing molecular anisotropy, one obtains $\mu_{\mathrm{proj}}=\mu^{*}_{\mathrm{RE}}$. Hence one expects the full ionic value of the rare earth moment to be measured. For very large r, i.e., huge magnetic anisotropy, the measured magnetic moment will only be half of the expected magnetic moment. Please note that this consideration is valid only for the case of the orbital magnetic moment. In the case of the spin moment the T_z term fully contributes to the experimentally determined effective spin moment.

The rare earth ions may alternatively exhibit an easy plane anisotropy instead of an easy axis anisotropy depending on the ligand field. The results of the corresponding calculations considering an easy plane anisotropy with anisotropy constant K are shown in Fig. 5(b). In this case μ^{*}_{RE} is larger than 0.71 independent on K and therefore larger than the experimental value for Dy(III). As Dy(III) and Tb(III) have a similar asymmetric shape of the $4f$ electron density, we conclude that the rare earth ions in $\{TbNi_5\}$ and $\{DyNi_5\}$ possess an easy axis anisotropy.

For the rare earth ions the expectation value of the dipole operator can be calculated exactly using the relation given in Ref. [54]. One obtains $T_z/S_z=-0.231,\ -0.111$, and -0.133 for Sm, Tb, and Dy, respectively. Please note that an atomic multiplet calculation results in different T_z values for the lighter rare earth ions [57]. For the heavier ions these differences are less than 10%. For consistency with the sum rules [Eq. (4)]

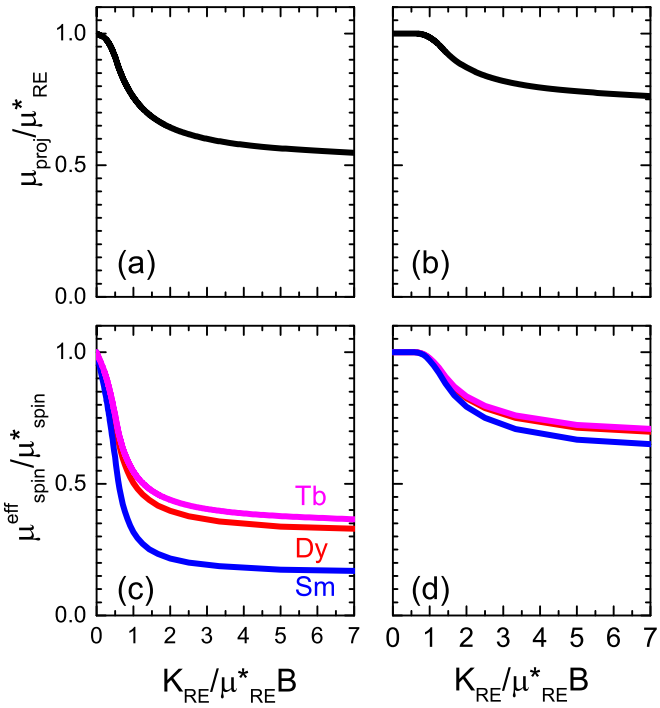

FIG. 5. Projected magnetic moment along the external field axis normalized to the absolute moment as a function of the ratio of anisotropy constant and Zeeman energy [see Eq. (4)] for the case of an easy axis magnetic anisotropy (a) and easy plane anisotropy (b), respectively. Effective spin moment along the external field axis normalized to the absolute moment as a function of the ratio of anisotropy constant and Zeeman energy [see Eq. (5)] for the case of easy axis (c) and easy plane anisotropy (d), respectively. The contribution from the T_z term is considered according to the exact ionic value for the indicated rare earth ions.

we consider in the following the values given in Ref. [54]. When the spin moment shows along the molecular symmetry axis the effective spin moment resulting from the sum rules is given by $\mu^{\rm eff}_{\rm spin} = 2(S_z + 3T_z)\mu_{\rm B}$. The measured effective spin moment is smaller than the spin moment because of the negative sign of T_z. If the direction of the spin moment deviates from the molecular symmetry axis by an angle $\delta = \theta - \vartheta$, the expectation value is given by $T_z(\delta) = T_z(3\cos^2\delta - 1)/2$. For negligible anisotropy, one obtains $\delta = \theta$ and the powder average results in a vanishing T_z contribution. For finite anisotropy we calculate the projected effective spin moment with respect to the absolute spin moment according to

$$\frac{\mu^{\rm eff}_{\rm spin}}{\mu^{*}_{\rm spin}} = \int_0^{\frac{\pi}{2}} \left(1 + 3\frac{T_z}{S_z}\right) \times \frac{3\cos^2[\theta - \vartheta(r)] - 1}{2} \cos\vartheta(r)\sin\theta\, d\theta. \quad (5)$$

The result of this calculation is shown in Figs. 5(c) and 5(d) for the case of an easy axis and easy plane anisotropy, respectively.

We now use this result to extract the absolute spin moments of the rare earth ions from the sum rule data. Assuming that the external field of 7 T is sufficient to saturate the magnetic moments against thermal fluctuations, which is certainly not true in the case of Sm, but may hold for Tb and Dy, we start from the orbital moment that is not changed by T_z. In the case of Dy, the experimentally obtained value is just 54(2)% of the ionic value. From Fig. 5(a) we thus obtain a ratio $r = 7(3)$. For the case of Tb the corresponding value is $r = 1.3(3)$. Because the spin orbit coupling aligns the spin and orbital moment, the same ratio r holds for the spin moment, too. Using the result of Fig. 5(c) we obtain a correction factor for the spin moment. Accordingly, the spin moment of Dy is given by $\mu_{\rm spin} = 6.0\,\mu_{\rm B}$, being close to the expected value of $5\mu_{\rm B}$. For the case of Tb one obtains a spin moment of $\mu_{\rm spin} = 6.2\,\mu_{\rm B}$, which almost exactly equals the expected value. The agreement of the spin moment with the corresponding ionic values justifies the model assumptions.

For the calculation of the molecular moment $\mu_{\rm mol}$ as measured by standard magnetometry we consider the sum of the Ni spin and orbital moment multiplied by $N = 5$ according to the chemical structure of the molecule. The contribution from the rare earth orbital moment is the same as measured by XMCD. Its spin moment, however, is larger compared to the measured XMCD value according to the contribution of the T_z term as discussed above. Here, we apply the corresponding correction factor from the ratio of $\mu_{\rm proj}(r)/\mu^*_{\rm RE}$ and $\mu^{\rm eff}_{\rm spin}(r)/\mu^*_{\rm spin}$ according to Eqs. (4) and (5). The result of the projected molecular moments is summarized in Table I for the case of Tb and Dy. We find a less good agreement with the molecular moment as determined by SQUID magnetometry. Values from SQUID magnetometry are smaller compared to the XMCD value. In this case, however, an error in the determination of the orbital moment of about 20% leads already to a considerable change of the T_z correction factors and thus may explain part of the discrepancy.

Important information directly results from the ratio r. For the case of Dy we have $r = 7(3)$ with $\mu^*_{\rm RE} = 10\,\mu_{\rm B}$. Hence the magnetic anisotropy constant equals $K_{\rm RE}({\rm Dy}) = 28(12)$ meV. A similar consideration for the case of Tb leads to $K_{\rm RE}({\rm Tb}) = 6.5(2.0)$ meV. Thus for both cases the magnetic anisotropy is remarkably large. For the case of Dy it even exceeds room temperature in thermal units.

A comparison of $\mu_{\rm SQUID}(H, T)$ with a spin-Hamiltonian model, considering the random orientation and representing the Dy(III) [Tb(III)] magnetic moment by a spin state of $S = 15/2$ [$S = 12/2$ in the case of Tb(III)] and the magnetic anisotropy by the corresponding anisotropy parameter $K = DS_z^2$, reveals a good agreement with the experimental data (Fig. 3). The fit to the experimental data results in an effective g value of $g = 1.41$ ($g = 1.67$). The spin-Hamiltonian model also considers the contribution of the Ni(II) moments. From the magnetometry results for $\{SmNi_5\}$ we conclude that the Ni(II) and the Sm(III) moment linearly increases with the magnetic field. As the magnetic moment determined by magnetometry closely agrees with the Ni(II) XMCD moment, we furthermore conclude that the Sm(III) moment is small. As a consequence, it is the Ni(II) magnetic moment contribution that increases almost linearly with external field. The value found for a 7 T field does not depend much on temperature in the range of 2 K to 10 K, i.e., the variation is less than 10%. This linear increase, instead of a Brillouin function behavior, might be explained by an antiferromagnetic coupling between neighboring Ni(II) spins. The Ni(II) magnetic moment has to be included in the fitting procedure for the magnetometry data for $TbNi_5$

and $DyNi_5$. Furthermore, the value for the Ni(II) moment is strongly correlated with the magnetic anisotropy value and therefore it is not possible to deduce the anisotropy parameter from the magnetometry data alone.

V. SUMMARY

Element-specific magnetic moments of $3d$-$4f$ heteronuclear 15-MC-5 $\{RENI_5\}$ metallacrowns have been determined using XMCD for powder samples. We have found comparatively small Ni(II) moments, which are explained by an intramolecular antiferromagnetic exchange coupling. For the case of Sm(III) we find an antiparallel alignment of rare earth and transition metal spin moment suggesting an antiferromagnetic exchange coupling. The Tb(III) and Dy(III) magnetic moments are aligned parallel to the Ni(II) moments. The rare earth magnetic moments are smaller than the corresponding ionic values resulting from Hund's rules in agreement with previous investigations of magnetic moments in molecules comprising RE(III) ions. The reduction of the magnetic moments is usually explained by a large magnetic anisotropy. We have exploited the ratio of the experimentally determined rare earth moment and the expected ionic value in order to determine the easy axis magnetic anisotropy. Considering the powder average this results in a magnetic anisotropy of 28 meV (340 K) in the case of Dy(III) and 7 meV (85 K) in the case of Tb(III). The magnetic anisotropy analysis of the Tb(III) and Dy(III) magnetic spin and orbital moments determined by the XMCD sum rules can be applied also for further $4f$ SMMs.

ACKNOWLEDGMENTS

Excellent support by the staff of BESSY II is gratefully acknowledged. This work is supported by the German Research Foundation (DFG) through the Transregional Collaborative Research Center SFB/TRR173 Spin+X, Projects A09. Financial support for developing and building the PM2-VEKMAG beamline and VEKMAG end station was provided by HZB and Federal Ministry of Education and Research (Bundesministerium für Bildung und Forschung) (Grants No. 05K10PC2, No. 05K10WR1, and No. 05K10KE1), respectively. Steffen Rudorff is acknowledged for technical support.

[1] A. Caneschi, D. Gatteschi, R. Sessoli, A. L. Barra, L. C. Brunel, and M. Guillot, J. Am. Chem. Soc. **113**, 5873 (1991).
[2] R. Sessoli, D. Gatteschi, A. Caneschi, and M. A. Novak, Nature (London) **365**, 141 (1993).
[3] D. Gatteschi, A. Caneschi, L. Pardi, and R. Sessoli, Science **265**, 1054 (1994).
[4] C. Cadiou, M. Murrie, C. Paulsen, V. Villar, W. Wernsdorfer, and R. E. P. Winpenny, Chem. Commun. **24**, 2666 (2001).
[5] J. J. Sokol, A. G. Hee, and J. R. Long, J. Am. Chem. Soc. **124**, 7656 (2002).
[6] C. J. Milios, R. Inglis, A. Vinslava, R. Bagai, W. Wernsdorfer, S. Parsons, S. P. Perlepes, G. Christou, and E. K. Brechin, J. Am. Chem. Soc. **129**, 12505 (2007).
[7] O. Waldmann, Inorg. Chem. **46**, 10035 (2007).
[8] E. Ruiz, J. Cirera, J. Cano, S. Alvarez, C. Loose, and J. Kortus, Chem. Commun. **1**, 52 (2008).
[9] R. Sessoli and A. K. Powell, Coord. Chem. **253**, 2328 (2009).
[10] L. Sorace, C. Benelli, and D. Gatteschi, Chem. Soc. Rev. **40**, 3092 (2011).
[11] N. Ishikawa, M. Sugita, T. Ishikawa, S. Koshihara, and Y. Kaizu, J. Am. Chem. Soc. **125**, 8694 (2003).
[12] M. A. AlDamen, J. M. Clemente-Juan, E. Coronado, C. Marti-Gastaldo, and A. Gaita-Arino, J. Am. Chem. Soc. **130**, 8874 (2008).
[13] M. A. AlDamen, S. Cardona-Serra, J. M. Clemente-Juan, E. Coronado, A. Gaita-Arino, C. Marti-Gastaldo, F. Luis, and O. Montero, Inorg. Chem. **48**, 3467 (2009).
[14] S.-D. Jiang, B.-W. Wang, H.-L. Sun, Z.-M. Wang, and S. Gao, J. Am. Chem. Soc. **133**, 4730 (2011).
[15] B. M. Guo, M. Day, Y.-C. Chen, M.-L. Tong, A. Mansikkamaki, and R. A. Layfield, Angew. Chem., Int. Ed. Engl. **56**, 11445 (2017).
[16] C. A. P. Goodwin, F. Orto, D. Reta, N. F. Chilton, and D. P. Millis, Nature (London) **548**, 439 (2017).
[17] R. Giraud, W. Wernsdorfer, A. M. Tkachuk, D. Mailly, and B. Barbara, Phys. Rev. Lett. **87**, 057203 (2001).
[18] P.-H. Lin, T. J. Burchell, L. Ungur, L. F. Chibotaru, W. Wernsdorfer, and M. Murugesu, Angew. Chem., Int. Ed. Engl. **48**, 9489 (2009).
[19] I. J. Hewitt, J. Tang, N. T. Madhu, C. E. Anson, Y. Lan, J. Luzon, M. Etienne, R. Sessoli, and A. K. Powell, Angew. Chem., Int. Ed. Engl. **49**, 6352 (2010).
[20] Y.-N. Guo, G.-F. Xu, P. Gamez, L. Zhao, S.-Y. Lin, R. Deng, J. Tang, and H.-J. Zhang, J. Am. Chem. Soc. **132**, 8538 (2010).
[21] R. J. Blagg, C. A. Muryn, E. J. L. McInnes, F. Tuna, and R. E. P. Winpenny, Angew. Chem., Int. Ed. Engl. **50**, 6530 (2011).
[22] J. Long, F. Habib, P.-H. Lin, I. Korobkov, G. Enright, L. Ungur, W. Wernsdorfer, L. F. Chibotaru, and M. Murugesu, J. Am. Chem. Soc. **133**, 5319 (2011).
[23] C. M. Zaleski, E. C. Depperman, J. W. Kampf, M. L. Kirk, and V. L. Pecoraro, Angew. Chem., Int. Ed. Engl. **43**, 3912 (2004).
[24] S. Osa, T. Kido, N. Matsumoto, N. Re, A. Pochaba, and J. Mrozinski, J. Am. Chem. Soc. **126**, 420 (2004).
[25] J. Rinck, G. Novitchi, W. Van den Heuvel, L. Ungur, Y. Lan, W. Wernsdorfer, C. E. Anson, L. F. Chibotaru, and A. K. Powell, Angew. Chem., Int. Ed. Engl. **49**, 7583 (2010).
[26] M. Holynska, D. Premuzic, I.-R. Jeon, W. Wernsdorfer, R. Clerac, and S. Dehnen, Chem.-Euro. J. **17**, 9605 (2011).
[27] J. Dreiser, K. S. Pedersen, C. Piamonteze, S. Rusponi, Z. Salman, M. E. Ali, M. Schau-Magnussen, C. A. Thuesen, S. Piligkos, H. Weihe, H. Mutka, O. Waldmann, P. Oppeneer, J. Bendix, F. Nolting, and H. Brune, Chem. Sci. **3**, 1024 (2012).
[28] P. Happ, C. Plenk, and E. Rentschler, Coord. Chem. Rev. **289**, 238 (2015).
[29] Q.-W. Li, J.-L. Liu, J.-H. Jia, Y.-C. Chen, J. Liu, L.-F. Wang, and M.-L. Tong, Chem. Commun. **51**, 10291 (2015).

[30] C. M. Zaleski, S. Tricard, E. C. Depperman, W. Wernsdorfer, T. Mallah, M. L. Kirk, and V. L. Pecoraro, Inorg. Chem. **50**, 11348 (2011).

[31] J. D. Rinehart and J. R. Long, Chem. Sci. **2**, 2078 (2011).

[32] W. W. Lukens and M. D. Walter, Inorg. Chem. **49**, 4458 (2010).

[33] N. Ishikawa, M. Sugita, T. Okubo, N. Tanaka, T. Lino, and Y. Kaizu, Inorg. Chem. **42**, 2440 (2003).

[34] J. Luzon, K. Bernot, I. J. Hewitt, C. E. Anson, A. K. Powell, and R. Sessoli, Phys. Rev. Lett. **100**, 247205 (2008).

[35] M. A. Arrio, A. Scuiller, P. Sainctavit, C. C. D. Moulin, T. Mallah, and M. Verdaguer, J. Am. Chem. Soc. **121**, 6414 (1999).

[36] G. Champion, N. Lalioti, V. Tangoulis, M. A. Arrio, P. Sainctavit, F. Villain, A. Caneschi, D. Gatteschi, C. Giorgetti, F. Baudelet, M. Verdaguer, and C. C. D. Moulin, J. Am. Chem. Soc. **125**, 8371 (2003).

[37] R. Moroni, Ch. Cartier dit Moulin, G. Champion, M. A. Arrio, Ph. Sainctavit, M. Verdaguer, and D. Gatteschi, Phys. Rev. B **68**, 064407 (2003).

[38] T. Hamamatsu, K. Yabe, M. Towatari, S. Osa, N. Matsumoto, N. Re, A. Pochaba, J. Mrozinski, J.-L. Gallani, A. Barla, P. Imperia, C. Paulsen, and J.-P. Kappler, Inorg. Chem. **46**, 4458 (2007).

[39] G. Rogez, B. Donnio, E. Terazzi, J.-L. Gallani, J.-P. Kappler, J.-P. Bucher, and M. Drillon, Adv. Mater. **21**, 4323 (2009).

[40] P. Gambardella, S. Stepanow, A. Dmitriev, J. Honolka, F. M. F. de Groot, M. Lingenfelder, S. Sen Gupta, D. D. Sarma, P. Bencok, S. Stanescu, S. Clair, S. Pons, N. Lin, A. P. Seitsonen, H. Brune, J. V. Barth, and K. Kern, Nat. Mater. **8**, 189 (2009).

[41] R. Biagi, J. Fernandez-Rodriguez, M. Gonidec, A. Mirone, V. Corradini, F. Moro, V. De Renzi, U. del Pennino, J. C. Cezar, D. B. Amabilino, and J. Veciana, Phys. Rev. B **82**, 224406 (2010).

[42] M. Mannini, F. Pineider, C. Danieli, F. Totti, L. Sorace, P. Sainctavit, M. A. Arrio, E. Otero, L. Joly, J. C. Cezar, A. Cornia, and R. Sessoli, Nature (London) **468**, 417 (2010).

[43] V. Corradini, A. Ghirri, U. del Pennino, R. Biagi, V. A. Milway, G. Timco, F. Tuna, R. E. P. Winpenny, and M. Affronte, Dalton Trans. **39**, 4928 (2010).

[44] S. Stepanow, J. Honolka, P. Gambardella, L. Vitali, N. Abdurakhmanova, T.-C. Tseng, S. Rauschenbach, S. L. Tait, V. Sessi, S. Klyatskaya, M. Ruben, and K. Kern, J. Am. Chem. Soc. **132**, 11900 (2010).

[45] M. Prinz, K. Kuepper, C. Taubitz, M. Raekers, S. Khanra, B. Biswas, T. Weyhermueller, M. Uhlarz, J. Wosnitza, J. Schnack, A. V. Postnikov, C. Schroeder, S. J. George, M. Neumann, and P. Chaudhuri, Inorg. Chem. **49**, 2093 (2010).

[46] M. Gonidec, R. Biagi, V. Corradini, F. Moro, V. De Renzi, U. del Pennino, D. Summa, L. Muccioli, C. Zannoni, D. B. Amabilino, and J. Veciana, J. Am. Chem. Soc. **133**, 6603 (2011).

[47] M. Mannini, E. Tancini, L. Sorace, P. Sainctavit, M.-A. Arrio, Y. Qian, E. Otero, D. Chiappe, L. Margheriti, J. C. Cezar, R. Sessoli, and A. Cornia, Inorg. Chem. **50**, 2911 (2011).

[48] A. Lodi Rizzini, C. Krull, T. Balashov, J. J. Kavich, A. Mugarza, P. S. Miedema, P. K. Thakur, V. Sessi, S. Klyatskaya, M. Ruben, S. Stepanow, and P. Gambardella, Phys. Rev. Lett. **107**, 177205 (2011).

[49] P. Stoll, M. Bernien, D. Rolf, F. Nickel, Q. Xu, C. Hartmann, T. R. Umbach, J. Kopprasch, J. N. Ladenthin, E. Schierle, E. Weschke, C. Czekelius, W. Kuch, and K. J. Franke, Phys. Rev. B **94**, 224426 (2016).

[50] P. Happ, A. Sapozhnik, J. Klanke, P. Czaja, A. Chernenkaya, K. Medjanik, S. Schuppler, P. Nagel, M. Merz, E. Rentschler, and H. J. Elmers, Phys. Rev. B **93**, 174404 (2016).

[51] P. Happ and E. Rentschler, Dalton Trans. **43**, 15308 (2014).

[52] J. L. S. H. Seda and J. Janczak, Inorg. Chem. Commun. **9**, 792 (2006).

[53] T. Noll and F. Radu, *Proceedings of the 9th Mechanical Engineering Design of Synchrotron Radiation Equipment and Instrumentation (MEDSI2016)* (JACoW, Geneva, Switzerland, 2017), pp. 370–373.

[54] P. Carra, B. T. Thole, M. Altarelli, and X. Wang, Phys. Rev. Lett. **70**, 694 (1993).

[55] B. T. Thole, P. Carra, F. Sette, and G. van der Laan, Phys. Rev. Lett. **68**, 1943 (1992).

[56] E. Stavitski and F. M. F. de Groot, Micron **41**, 687 (2010).

[57] Y. Teramura, A. Tanaka, and T. Jo, J. Phys. Soc. Jpn. **65**, 1053 (1996).

[58] Y. Teramura, A. Tanaka, and T. Jo, J. Phys. Soc. Jpn. **65**, 3056 (1996).

[59] G. Lorusso, V. Corradini, A. Candini, A. Ghirri, R. Biagi, U. del Pennino, S. Carretta, E. Garlatti, P. Santini, G. Amoretti, G. Timco, R. E. P. Winpenny, and M. Affronte, Phys. Rev. B **82**, 144420 (2010).

[60] J. P. Crocombette, B. T. Thole, and F. Jollet, J. Phys.: Condens. Matter **8**, 4095 (1996).

[61] S. Stepanow, A. Mugarza, G. Ceballos, P. Moras, J. C. Cezar, C. Carbone, and P. Gambardella, Phys. Rev. B **82**, 014405 (2010).

[62] J. Stohr, J. Electron. Spectrosc. Relat. Phenom. **75**, 253 (1995).

[63] B. T. Thole and G. van der Laan, Phys. Rev. B **38**, 3158 (1988).

[64] S. K. Singh, M. F. Beg, and G. Rajaraman, Chemistry **22**, 672 (2016).

[65] B. Sanyal, C. Antoniak, T. Burkert, B. Krumme, A. Warland, F. Stromberg, C. Praetorius, K. Fauth, H. Wende, and O. Eriksson, Phys. Rev. Lett. **104**, 156402 (2010).